

PFC/JA-94-39

Active Millimeter-Wave Pyrometer
P. P. Woskov, D. R. Cohn, D. Y. Rhee, P. Thomas,
C. H. Titus¹, and J. E. Surma²

Plasma Fusion Center
Massachusetts Institute of Technology
Cambridge, MA 02139

December 1994

Submitted to *Review of Scientific Instruments*.

Supported by Buried Waste Integrated Demonstration, Office of Technology Development, Environmental Demonstration and Waste Management, U. S. Department of Energy through Battelle - Pacific Northwest Laboratories Contract No. 154462-A-L2.

¹T & R Associates, Wayne, PA 19087

²Pacific Northwest Laboratories, Richland, WA 99352

Active Millimeter-Wave Pyrometer

P. P. Woskov, D. R. Cohn, D. Y. Rhee, and P. Thomas
Plasma Fusion Center, Massachusetts Institute of Technology, Cambridge, MA 02139

C. H. Titus
T&R Associates, Wayne, PA 19087

J. E. Surma
Pacific Northwest Laboratories, Richland, WA 99352

Abstract

A 135 GHz heterodyne receiver with a rotatable graphite waveguide/mirror system has been implemented on a waste remediation DC arc furnace for internal surface temperature measurements. The linear temperature measurement range extends from $<1^{\circ}$ to approximately $15,000^{\circ}\text{C}$ relative to ambient with a simultaneous capability to monitor surface reflectivity with the local oscillator leakage. Reliable and robust operation on a continuous 24 hour basis in a smoky, dirty furnace environment is demonstrated for a total of 5 furnace runs reaching a maximum temperature of 2200°C . Complete temperature profile measurements with approximately 5 cm spatial resolution clearly documented thermal gradients on the slag melt surface and refractory walls and ceiling for all operating regimes of the furnace. The unique active probing capability of this instrument provided additional real time information on melt surface turbulence, changing furnace wall emissivity, and millimeter-wave optic losses inside the furnace.

I. Introduction

There is a continuing need for reliable and accurate temperature measurements inside hot and dirty environments. Many processes encompassing manufacturing, waste remediation, and power production make use of high temperature furnaces where currently available temperature measurement instrumentation is not always adequate. Thermocouples require direct surface contact which is not often possible or practical and they are limited to temperatures $< 1700^{\circ}\text{C}$. Infrared pyrometers require clear, direct lines of sight that are frequently unavailable or become obscured during operations. Furthermore the surface emissivity, which can vary during the process, must be known. The active millimeter-wave pyrometer presented here makes a significant advance on these limitations. It is a robust furnace temperature measurement instrument with new capabilities for accessing hot, dirty environments and with a potential for simultaneously monitoring surface emissivity.

A large investment in the development of millimeter-wave radiometry for temperature measurements has already been made by big science programs. This technology is in routine use for the measurement of the $10^8\text{ }^{\circ}\text{C}$ temperatures inside Department of Energy (DOE) sponsored fusion energy plasma experiments [1] and has been used by NASA to study the 2.7 K cosmic background temperature [2]. Adapting this technology as described here will benefit many other scientific areas and processes of economical and environmental importance. An environmentally important one to which the active millimeter-wave pyrometer is applied here is the remediation of hazardous wastes. Results are presented for its use on Mark II, a pilot scale DC graphite arc furnace, being used at MIT for the investigation of treatment of wastes as part of DOE's Buried Waste Integrated Demonstration (BWID) [3].

The millimeter-wave range of the electromagnetic spectrum is ideally suited for pyrometry inside harsh furnace environments. These wavelengths are long enough to penetrate smoky atmospheres and otherwise optically obscured viewing paths, but still short enough for good spatial resolution. Also direct lines of sight to the furnace surfaces to be monitored are not required since millimeter-wave waveguides and mirrors can be made of refractory materials and implemented inside the furnace. This capability is also useful for minimizing the number of furnace penetrations needed to obtain complete monitoring coverage of the internal surfaces. In fact, with one small penetration it was possible to obtain complete vertical profile temperature measurements inside Mark II by a simple rotation of an internal mirror.

Another unique feature of this pyrometer is that it is active. The very nature of a millimeter-wave heterodyne receiver makes possible active probing without any special modification to the receiver electronics. Any heterodyne receiver naturally leaks out the local oscillator signal. Normally this is considered wasted signal and in some cases a nuisance interference signal to other electronics, but here we take advantage of this leaked oscillator signal to provide for an active probing capability. The reflection of this probe beam provides information that can be used to keep the

temperature measurement calibrated throughout the operating range of the furnace including a potential for real time surface emissivity measurements via surface reflection. When viewing down into the hearth this reflection signal provided additional information on melt surface fluctuations which could be a useful indicator of the slag melt chemistry and waste loading operations.

II. Analytic Basis

A heterodyne receiver pyrometer produces a voltage signal that is directly proportional to the thermal power radiated by a surface filling the pyrometer field-of-view. In the millimeter-wave range of the electromagnetic spectrum the radiated thermal power, in turn, is linearly related to the temperature through Boltzmann's constant, k_B , as [4]:

$$P_s = k_B \Delta f T_s \quad (1)$$

where Δf is the frequency bandwidth over which the signal is detected and T_s is the surface temperature. This is in sharp contrast to infrared pyrometers which operate on or near the peak of the black-body curve where the thermal energy detected is proportional to the fourth power of the surface temperature [5]. Millimeter-wave pyrometers therefore have another advantage over their infrared counterparts in that a single instrument can have a much larger dynamic range for temperature measurements.

The voltage signal output from a heterodyne receiver pyrometer is determined not only by the temperature of the surface that fills its field-of-view, but also by its own internal noise temperature. If a room temperature black-body is placed directly in front of the receiver field-of-view, then the voltage output signal can be expressed as:

$$V_r = C k_B \Delta f (T_p + T_r) \quad (2)$$

where T_p is the pyrometer noise temperature, T_r is room temperature, and C is a proportionality constant depending on the pyrometer gain and power to voltage response. A similar equation can be written for the case when a black-body calibration source is placed in front of the pyrometer field-of-view:

$$V_c = C k_B \Delta f (T_p + T_c) \quad (3)$$

where T_c is the temperature of the calibration source which for the present measurements was liquid nitrogen cooled at 77 K.

The voltage signal when the pyrometer views the inside furnace surfaces through a window, waveguide, and via reflection off an internal mirror is more complicated. One must take into account all the signal transmission losses of these components as well as the thermal radiation contributions of these components to the total signal. Figure 1 illustrates this case. The corresponding equation for the voltage signal is given by:

$$V_s = Ck_B\Delta f(T_p + \epsilon_w T_w + \tau_w \epsilon_m T_m + \tau_w \tau_m \epsilon_s T_s) \quad (4)$$

where ϵ_w , T_w , ϵ_m , T_m , ϵ_s , and T_s are the emissivities and temperatures of the window/waveguide, mirror, and viewed surface, respectively and τ_w and τ_m are the transmission factors for the window/waveguide and mirror, respectively. The window is treated here as part of the waveguide and not separately because laboratory measurements have shown the Teflon window losses in the present instrument to be very small (<2%). Also note that the transmission factor for the mirror is via reflection.

The second term on the right of Equation (4) represents the signal contribution of the window/waveguide, the third term represents the signal contribution of the mirror as reduced by the transmission factor through the window/waveguide, and the fourth term is the viewed surface signal as reduced by the mirror and window/waveguide losses. It is assumed here that there are no additional signal losses or contributions from the atmospheric propagation path between the mirror and viewed surface. This is believed to be a good assumption because of the penetration capability of millimeter wavelengths in smoky environments and the short propagation path lengths of less than 1 meter in the present setup.

The emissivity and transmission factor of each component are related if we make the assumption that the part of the signal incident on the component but not transmitted is absorbed by that component. Applying Kirchhoff's law which equates absorption and emissivity gives the following relation between emissivity and transmission:

$$\tau_x = 1 - \epsilon_x \quad (5)$$

This relation can be used to determine the emissivities of the transmission line components from measurements of transmission losses.

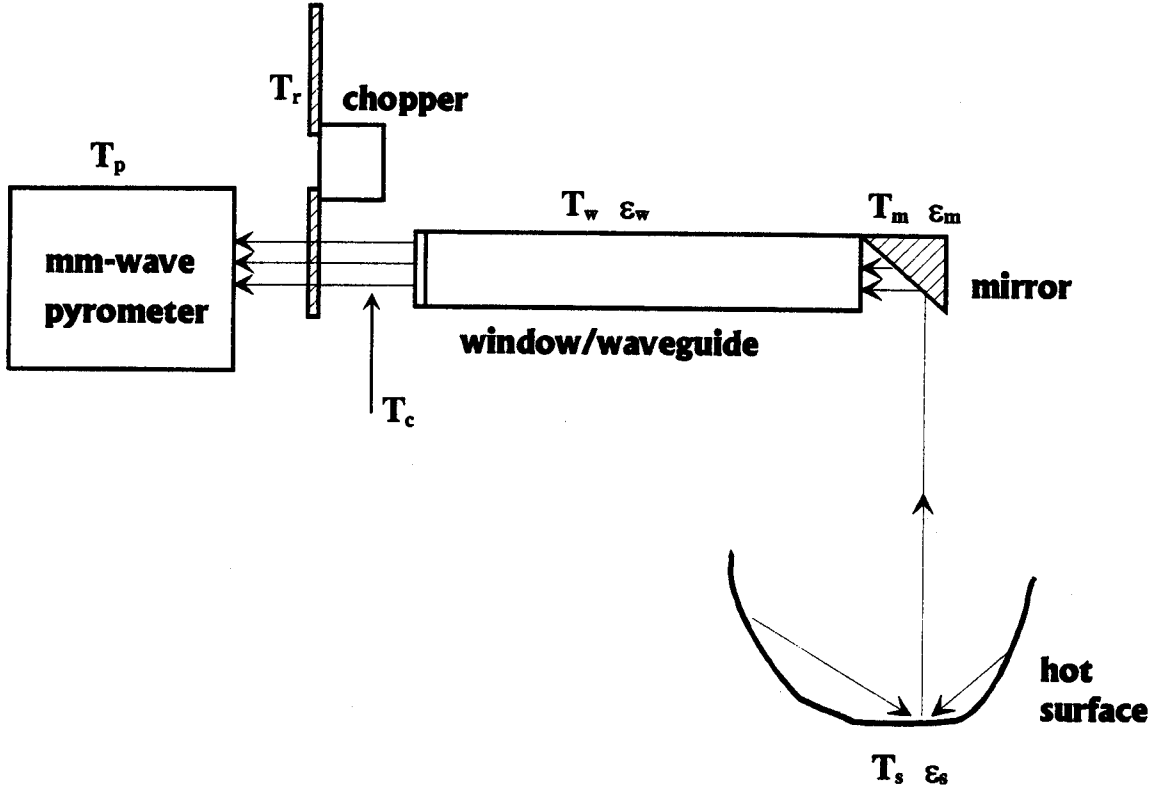


Figure 1. Illustration of the major elements in the millimeter-wave setup contributing signal to the pyrometer.

In a practical measurement situation, difference voltages are measured. The chopper in Figure 1 is rotating and a lock-in amplifier, referenced to the chopper frequency, measures the difference signal between the room temperature black-body on the chopper blades and the signal when the blades unblock the receiver field-of-view. A calibration difference signal is obtained when a calibrating black-body is located behind the chopper. This signal is given by subtracting Equation (3) from Equation (2):

$$V_{cal} = V_r - V_c = Ck_B \Delta f (T_r - T_c) \quad (6)$$

The temperature measurement difference signal of interest is obtained by subtracting Equation (2) from Equation (4):

$$V_{sig} = V_s - V_r = Ck_B \Delta f (\epsilon_w T_w + \tau_w \epsilon_m T_m + \tau_w \tau_m \epsilon_s T_s - T_r) \quad (7)$$

Examination of Equations 6 and 7 shows that the need to know the receiver noise temperature drops out when using difference signals. Furthermore, taking the ratio of Equation 7 to 6 eliminates the need to know the common constant factors. This is strictly true only if the total thermal signal is less than the receiver noise temperature. Otherwise the nonlinear response of the receiver detector diode would need to be considered. Solving Equations 6 and 7 for the viewed surface temperature gives:

$$T_s = \frac{V_{sig} (T_r - T_c)}{V_{cal} \tau_w \tau_m \epsilon_s} - \frac{\epsilon_w}{\tau_w \tau_m \epsilon_s} T_w - \frac{\epsilon_m}{\tau_m \epsilon_s} T_m + \frac{1}{\tau_w \tau_m \epsilon_s} T_r \quad (8)$$

In order to determine the viewed surface temperature, the contributions to the total signal of the window/waveguide and mirror must be subtracted. In practice it is not always possible to determine the emissivities and temperatures of the transmission line components or internal furnace surfaces throughout the operating temperature range of the furnace. Also surface depositions and erosion inside the furnace complicate determinations of these parameters. Therefore Equation (8) was approximated for most of the routine data acquisition by:

$$T_s \cong \frac{V_{sig} (T_r - T_c)}{V_{cal} \tau} + T_r \quad (9)$$

where $\tau \geq \tau_w \tau_m$ is the total transmission factor that is erred on the high side to partially compensate for the signal contributions by the pyrometer transmission line components. This approximation is exact if all the transmission line losses are at room temperature.

The additional assumption in Equation (9) that $\epsilon_s \approx 1$ is justified because laboratory measurements have shown the emissivities of the exposed surfaces inside the furnace to be high and because the reflected part of the pyrometer field-of-view sees other hot surfaces. At the present pyrometer frequency of 135 GHz the emissivity of unmelted Idaho Falls soil used in the first Mark II waste fill tests was measured to be 0.99 and that of the high alumina content refractory surface used in the furnace walls and ceiling to be 0.88. The present furnace measurements do show that these emissivities have decreased as the soil has melted and as deposits have formed on the inside surfaces but the assumption that $\epsilon_s \approx 1$ should still be a reasonable first approximation due to the internal nature of the field-of-view reflections.

III. Millimeter-Wave Pyrometer Electronics

The details of the millimeter-wave heterodyne receiver used as the pyrometer are shown in Figure 2. A scalar horn with a diffraction limited free space Gaussian field-of-view collects the emission and reflected signals. A 3 dB directional coupler combines half the incident signals and half the local oscillator power and directs them to a mixer where the frequency difference signal is generated. The local oscillator (LO) is a 135.4 GHz tripled Gunn oscillator source. The intermediate frequency (IF) difference signal, which corresponds to the downshifted thermal emission, is amplified in the range of 0.4 to 1.5 GHz as determined by a high pass filter and the amplifier gain. The total IF gain is about 65 dB. A square law diode detector rectifies the IF signal and produces a voltage level that is proportional to power.

Part of the LO incident on the mixer is reflected by the mixer out the receiver horn and is used as the active probe beam. On reflection back to the mixer by the surface being viewed this signal mixes with itself and produces a dc level which is proportional to the surface reflection and the round trip transmission losses. The mixer dc level is monitored through a bias tee which is part of the circuit to dc bias the mixer to optimize its frequency down conversion efficiency. The small reflected dc signal is distinguishable from the much larger dc bias level because it is modulated by the chopper. A lock-in amplifier referenced to the chopper readily detects this signal.

The receiver noise temperature was measured to be approximately 15,000 K double sideband. The sidebands correspond to 133.9 - 135.0 GHz and 135.8 - 136.9 GHz above and below the LO. A high receiver noise temperature relative to the surface temperatures to be measured is a desirable feature for a millimeter-wave pyrometer because it insures that the voltage response will be a linear function of temperature. Otherwise the nonlinear response of the detector diode would be a factor. The small temperature signal imbedded in the large receiver background noise is readily detected with a lock-in amplifier referenced to the signal chopper. Very good temperature measurement sensitivity is possible with wide receiver bandwidth and sufficient time integration. The minimum detectable temperature rise is given by [6]:

$$\Delta T_{\min} = \frac{T_p}{\sqrt{t\Delta f}} \quad (10)$$

where T_p is the receiver noise temperature, t is the signal integration time, and Δf is the total receiver bandwidth. For our receiver bandwidth of 2.2 GHz and a one second signal integration time, this corresponds to a minimum detectable temperature change of approximately 0.3° C.

A computer acquires the lock-in amplifier signals and displays the temperature and reflection values in real time in a scrolling chart format. The computer calculates the temperature from the lock-in signal by using Eq. (9) with V_{cal} and τ values as determined by the calibration procedure described below. The linear temperature

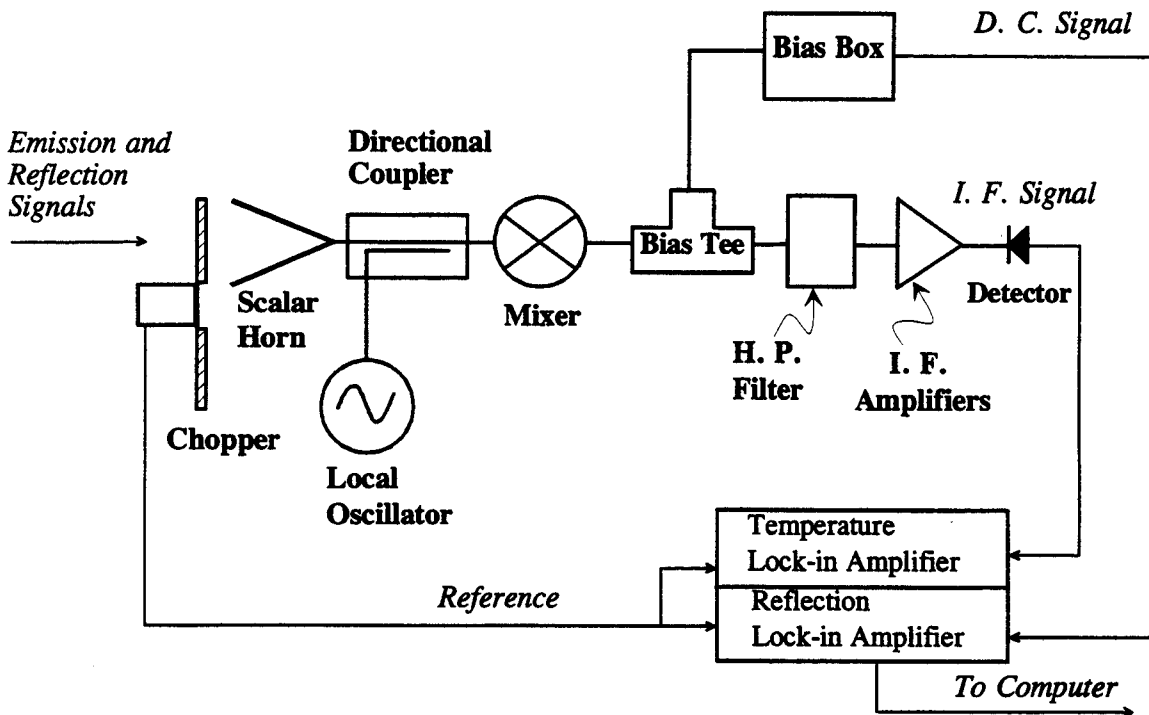


Figure 2. Block diagram of the millimeter-wave heterodyne receiver electronics for simultaneous measurement of the surface electromagnetic emission and local oscillator reflection.

measurement range of this instrument from $< 1^\circ$ to about $15,000^\circ$ C relative to ambient covers all furnace processes of interest.

IV. Experimental Setup on Mark II

Figure 3 shows the temperature measurement setup on Mark II. The furnace cross section is shown at the height of the pyrometer waveguide penetration into the furnace. The inner furnace chamber has a diameter of 91 cm and a height of 137 cm from the bottom of the hearth to the ceiling. The waveguide penetrates at a height of 97 cm above the hearth bottom in a direction that is offset from a radial line by 15 cm.

A unique feature of this furnace is the coaxial pair of graphite electrodes centered in the chamber which allows transfer and non transfer arc operation [3]. The outer electrode outer diameter is 41 cm leaving a maximum space of 25 cm between the inner furnace wall and the electrodes. The protrusion of the pyrometer waveguide into the furnace must be kept significantly less than this because the graphite electrodes are free to swing if hit by the waste feed. In the present setup the maximum extension of the waveguide into the furnace is 10 cm. A flat graphite mirror in the end of the waveguide directs the radiometer field-of-view sideways at a 90° angle to the axis of the guide as shown by the arrow in Figure 3.

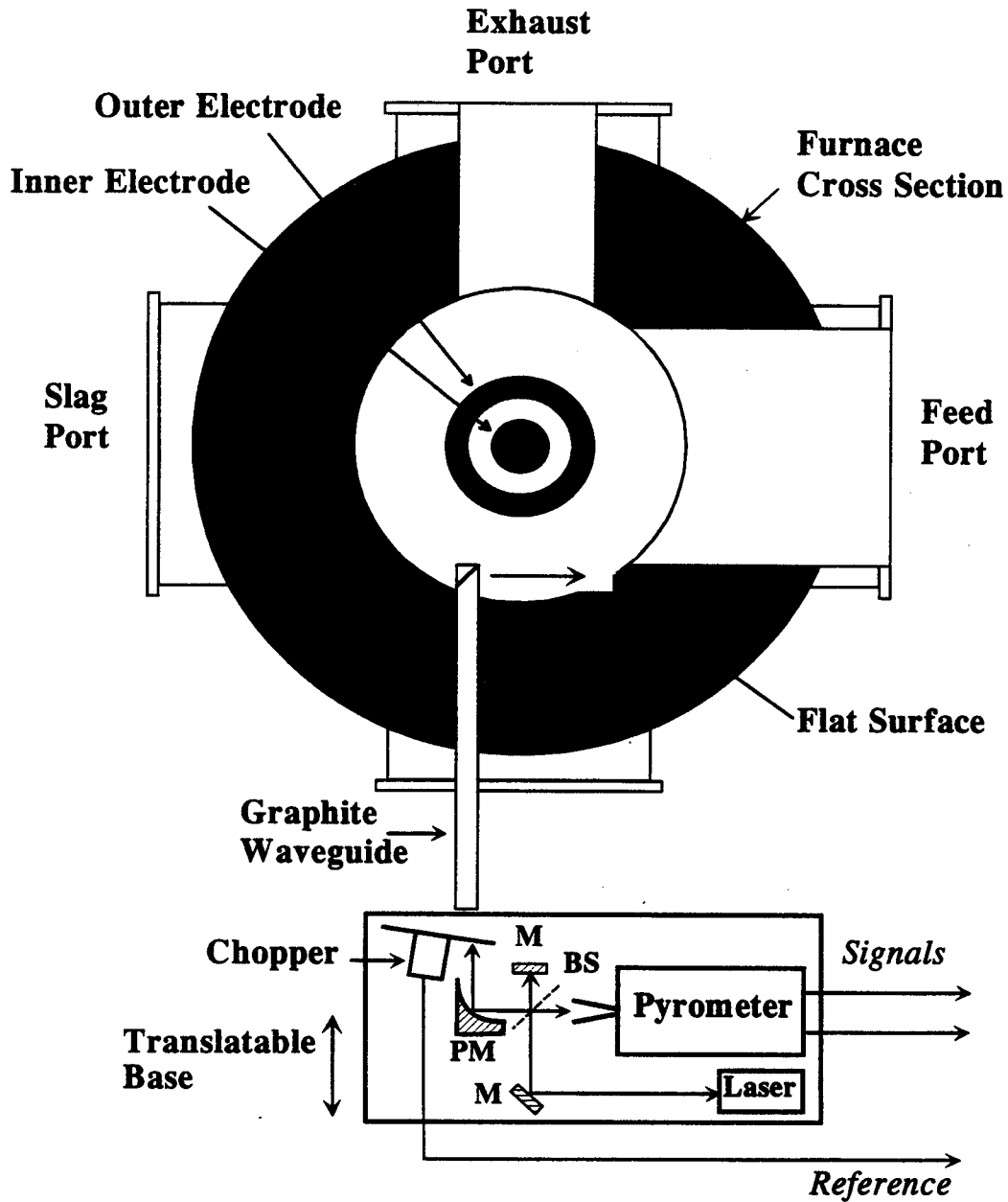


Figure 3. Millimeter-wave pyrometer temperature measurement setup in the Mark II furnace where M are flat mirrors, PM is an off-axis parabolic focusing mirror, and BS is a polyethylene beamsplitter.

The waveguide itself is a 3.8 cm inner diameter, 126 cm long, graphite tube which is corrugated on the inside to propagate the HE_{11} waveguide mode [7]. This waveguide mode is the most efficient one for waveguides greater than one wavelength in diameter. It is the key reason why it was possible to construct an efficient waveguide from graphite. Also, the HE_{11} mode launches as a free space Gaussian beam which provides efficient coupling to the receiver and the best diffraction limited

spatial resolution [8]. An alumina sleeve around the graphite and a Teflon window electrically insulate and seal the waveguide from the outside. Nitrogen gas purge through the waveguide prevents the inside of the waveguide from oxidizing during furnace operation. The furnace itself is also purged with nitrogen gas.

The pyrometer with the chopper and associated optics is located on a translatable platform. Translating the pyrometer system to change the signal path length is necessary when making reflection measurements because the fixed frequency probe beam is coherent. The reflection signal interference maxima and minima are mapped out by translation of several half wavelengths. Alternatively, the interference standing wave pattern could be mapped out by frequency sweeping the LO several 100 MHz but this was not implemented in the present set up because a leveled LO would be required. A 90° off-axis parabolic mirror is used to optimally couple the receiver field-of-view to the graphite waveguide. Translation by less than 1 cm does not noticeably affect this coupling. A visible laser beam can be superimposed on the pyrometer field-of-view by a polyethylene beamsplitter for alignment of the entire system.

The graphite waveguide is rotatable so that the radiometer field-of-view can be continuously scanned from looking up at the ceiling and down into the hearth. This is illustrated in Figure 4 where approximately 0° corresponds to looking straight up and approximately 180° straight down. For an angular viewing range from about 0° to 45° the view is of the ceiling. For an angular viewing range from about 145° to 195° the view is of the hearth and its fill. Actually the viewing locations are not as sharply defined as implied by Figure 4 because the field-of-view spot size is not a point. Only the center of the viewing spot intersection with the furnace surface is shown.

The spatial resolution of the radiometer depends on the distance of the viewed surface from the waveguide. For a distance of 40 cm, which is approximately the distance to the ceiling and wall for viewing directions of 0° and 90°, respectively, the $1/e^2$ spot size (the diameter within which 87% of a Gaussian profile is contained) is about 5 cm. The furthest distance is to the bottom of the hearth, 97 cm, where the $1/e^2$ spot size is 12 cm. More typically, the hearth has a fill and the spatial resolution is about 5-7 cm to the top of this fill.

V. Calibration

The response of the radiometer to temperature differences, and the signal losses in the waveguide transmission system were calibrated with a liquid nitrogen cooled black-body. The radiometer responds to hot or cold temperature differences relative to the chopper blade reference. A liquid nitrogen cooled black-body source of extended dimensions which fills the entire radiometer field-of-view can be readily obtained and provides an accurately known temperature of 77 K for calibration. Commercially available Eccosorb™ [9], a millimeter-wave absorbing foam plastic, was used as the black-body material and also covered the chopper blades. The calibration procedure

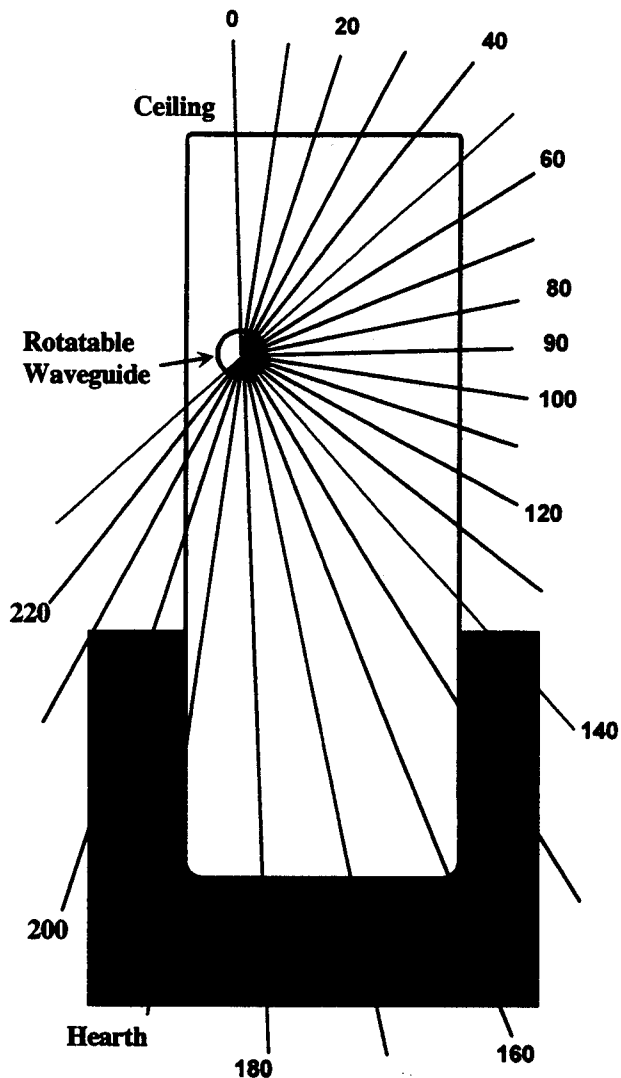


Figure 4. Pyrometer view directions and approximate intersection with the inside furnace surfaces.

involved alternately holding a room temperature and then a liquid nitrogen cooled sheet of Eccosorb in the radiometer field-of-view behind the chopper. The room temperature measurement was used to determine the zero offset signal. The cold temperature measurement determined the response to a known temperature, signal V_{cal} of Eq. (9). The calibration to the outside of the graphite waveguide could be checked at any time during furnace operation.

The signal losses due to the graphite waveguide, mirror, and Teflon window were determined by comparing cold black-body measurements at the outside of the furnace to those made inside the furnace when the furnace was open between runs. The total transmission was measured to be 0.89 ± 0.02 when the waveguide system was new. Most of the transmission losses are due to the waveguide itself. Window losses, which were minimized by window surface rulings [10], and graphite mirror

reflectivity losses were each determined to account for no more than 2% of the total losses. Theoretical calculations showed that the waveguide losses also should have been less than 1% for the HE_{11} mode in this length of graphite guide, but probably were higher because the present waveguide did not have perfect unbroken corrugations throughout its length. Nevertheless, using the value of 0.89 for τ in Eq. (9) would cause very little error in the temperature determination even at high temperature because the losses are distributed across the entire waveguide system with very little of it at high temperature to contribute to the temperature signal.

Unfortunately, it was found that the waveguide system transmission losses would increase during a furnace run largely due to surface corrosion of the graphite mirror inside the furnace. Therefore, the determination of the correct value of τ to use in Eq. (9) is the greatest uncertainty in the present calibration. Degradation of the reflectivity of the internal furnace mirror during furnace operation, however, is not as detrimental on the pyrometer calibration as it would first seem. This is because the mirror is hot and what it loses in decreased reflectivity it largely makes up by its concurrent increase in emission. Evaluation of the temperature measurements using the full Eq. (8) after a furnace run when temperature profile and transmission loss measurements are available to determine ϵ_w , T_w , ϵ_m , and T_m show that in most cases the approximate Eq. (9) is in error by only a few percent even when the graphite mirror reflectivity has decreased by up to 20%, as was observed for one of the furnace runs. The error is always in the direction that the measured temperature is too high which is the desirable direction for the calibration to fail making it unlikely the furnace could be overheated.

VI. Measurements

At the time of this writing the active millimeter-wave pyrometer was used in five high power runs of Mark II after an initial low power test [11]. Table 1 summarizes the length of the runs and the maximum temperatures achieved. The pyrometer was operational on a 24 hour basis throughout these run periods plus two to four days additional after furnace shut down to monitor cool down. The furnace started out with a carbon pile resistor consisting of alternating layers of steel plates and coke stacked in the center of the hearth for initial warm up by joule heating. The remains of this resistor were still useable up to the start of Run #5. Clean Idaho Falls soil with a 10% mix by weight of calcium carbonate to improve initial glass melt flow filled the hearth around the carbon pile resistor.

The first two runs were long slow warm ups to condition the refractory furnace interior. Runs #2, 3, and 5 achieved glass melt temperatures. On Run #5 approximately 750 pounds of soil was loaded while the furnace was at temperature and glass was successfully poured. The millimeter-wave pyrometer operated well throughout all these runs. In fact, it was the primary diagnostic relied upon to control the furnace power.

Table 1. Summary of High-Power Mark II Runs

Run Number	Run Length (Days)	Maximum Temperature (°C)
#1	11	960
#2	10	2200
#3	5	1450
#4	1	725
#5	3	1640

Illustrative signals obtained from this pyrometer are shown in Figure 5. The temperature and reflection signal records for day 4 of Run #5 are plotted from midnight to midnight. These signals were recorded once every six seconds. Gaps in the plots correspond to times when the pyrometer field-of-view was rotated away from the directions indicated to obtain temperature profile or reflection measurements at other locations.

Day 4 was the final day of Run #5 after the first soil filling of the hearth the previous day. The furnace arc power was reduced through the night and early morning to maintain a temperature near 1200° C. After 8:00 hours the arc power was increased to increase the melt temperature above 1450° C to prepare for the second campaign of soil loading. The pyrometer view was also moved to 190° to better monitor the temperature of the melt near the spout. During the soil loading the melt was purposely superheated to temperatures >1600° C, as guided by the pyrometer, in an attempt to minimize glass freezing at the end of the pour spout.

Soil was loaded into Mark II through air lock chambers in 40 pound paper bags which were dropped into the hearth at 7 to 27 minute intervals. Note that during soil loading, which is known to be a particularly smoky time inside the furnace, the temperature signal is not significantly perturbed. However, when the pyrometer view is turned more toward the load port as was done on day 3 of Run #5 during the first soil loading campaign (not shown) decreases in melt surface temperature were observed as each soil bag was dropped into the hearth. Apparently, the observations on day 4 indicate that by the time the newly loaded soil has mixed and drifted toward the spout side of the hearth it has largely equilibrated with the melt or is no longer on the surface.

After completing the second loading campaign with six soil bags the melt temperature was allowed to decrease. Just before furnace shut down at approximately 10:45 hours the arc length and power were briefly increased for resistivity measurements, producing the spike in the temperature record. After power shut down the furnace generally cooled off exponentially with deviations from exponential behavior attributable to changes in the furnace nitrogen gas purge. The pyrometer view is also rotated to view the edge of the hearth at 155° because this is the hottest point during cool down.

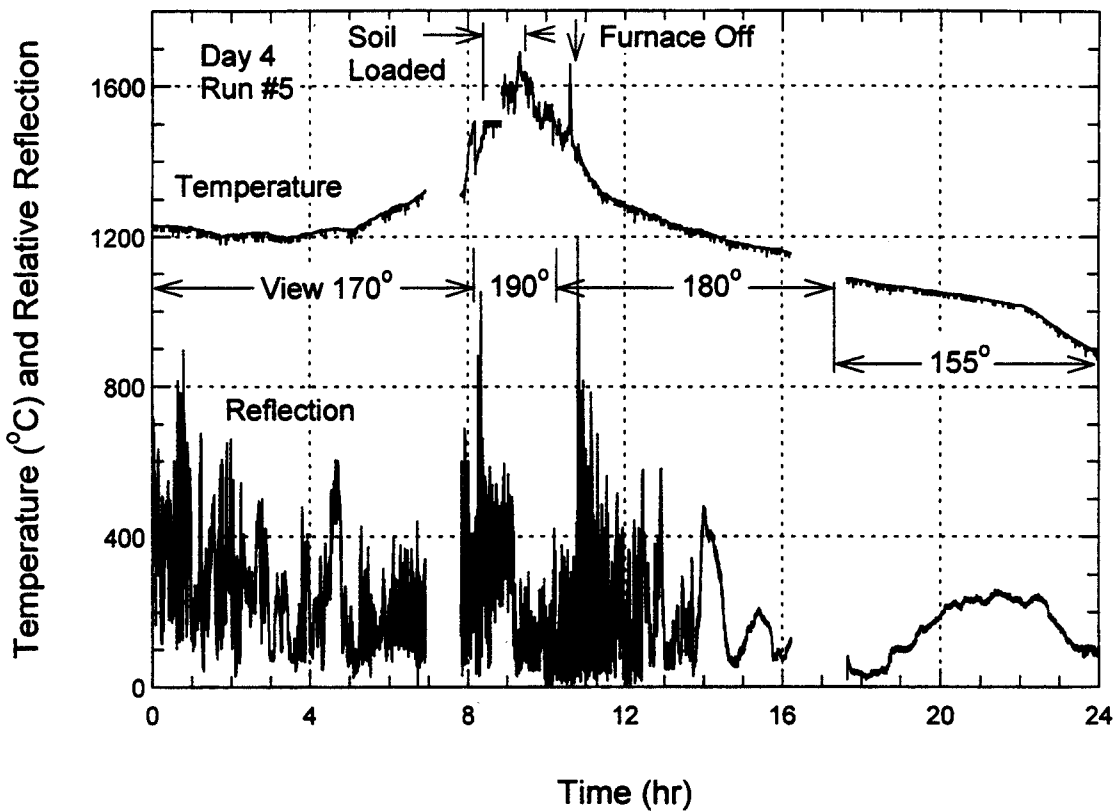


Figure 5. Temperature and reflection signal for the fourth day of Run #5 in the Mark II furnace.

Rapid temperature rises of hundreds of degrees centigrade on less than minute time scales, similar to the temperature spike near furnace shut down in Figure 5, were observed with small changes in arc power and length on other furnace run days. It was first thought that these high temperatures were not true surface temperatures inside the furnace but arc emission somehow directly or indirectly detected by the pyrometer. However, after Run #2 when 2200° C temperatures were briefly recorded it was found that some of the 1.9 cm diameter alumina rods (melting temperature 2015° C) that were part of a weir in the slag pour port were completely melted away. This corroborated the high surface temperatures observed with the millimeter-wave pyrometer. After Run #2 the pyrometer temperature signal was used to keep the arc under control and further melting of the remaining alumina rods was not observed.

VI. Reflection Measurements

The active probing capability of this pyrometer provides additional unique information on the condition of the internal furnace surfaces and on the performance of the pyrometer. The lower trace in Fig. 5 shows the simultaneous return reflection

from the surface registering the temperature in the upper trace. When viewing into the hearth large fluctuations in the reflected signal tend to increase in frequency and amplitude with higher temperatures as the melt apparently becomes more fluid. This is well illustrated by the first few hours of cool down after the furnace is shut off. As the melt cools down the reflection signal fluctuations decrease in amplitude and frequency and then make a sudden transition to a smoothly varying return signal as the temperature drops below 1000° C. A similar sharp transition in the reflection signal was not observed during warm up of the initial soil fill, though there was about an order of magnitude difference in the signals between the lower and highest temperatures. These observations are not quantitative, but do confirm that the pyrometer has a clear view of the inside surfaces throughout a furnace run and provide an indication of the chemistry in the melt which with further study might be useful for furnace control.

Our original goal for the active probing capability of the pyrometer, as a real time monitor of surface emissivity, requires quantitative measurements. In order to have a quantitative reflection measurement the surface being viewed must be orientated to direct the reflection back to the pyrometer. This is possible only for three viewing directions inside Mark II: viewing up at the ceiling, viewing sideways at a flat surface molded into the wall for this purpose as shown in Fig. 3, and looking straight down at the melt. In addition, the pyrometer must be translated to account for the standing wave pattern in the reflection signal due to the coherent interference between the transmitted and reflected probe beam.

Figure 6 shows typical return signals for the three view directions in Mark II where a direct return signal is expected. These signals were recorded prior to the start of Run #3. The standing wave pattern is shown for each view direction as the pyrometer was slowly translated. Two peaks are produced for each wavelength of translation (2.2 mm). A change in signal path length of only 1.1 mm is sufficient to cause the reflection to fluctuate from a minimum to a maximum value. The ceiling provides the strongest return signal followed by the wall, with the weakest return from the unmelted fill in the hearth. The rotatable waveguide/mirror was carefully adjusted for get the maximum standing wave pattern in each direction, though there wasn't a critical dependence on alignment when viewing down into the hearth. Reflection measurements such as these were made periodically throughout the furnace runs and the peaks of the standing wave pattern were averaged and plotted to determine if quantitative changes in surface reflectivity could be measured.

Figure 7 shows the results for the wall reflectivity measurements for Run #3 superimposed on the partially smoothed temperature record for that run. The pyrometer looked into the hearth for most of the run, but some of the structure in the temperature record is due to viewing other cooler surfaces. The major cool down feature starting at about day 1.7 was due to furnace shut down to make a minor repair in the soil loading system. The furnace was restarted at about day 2.8. The wall reflection signal shows a small increase at the start of the run and then decreases as the temperature in the hearth increases past 700° C. Just before the furnace was restarted

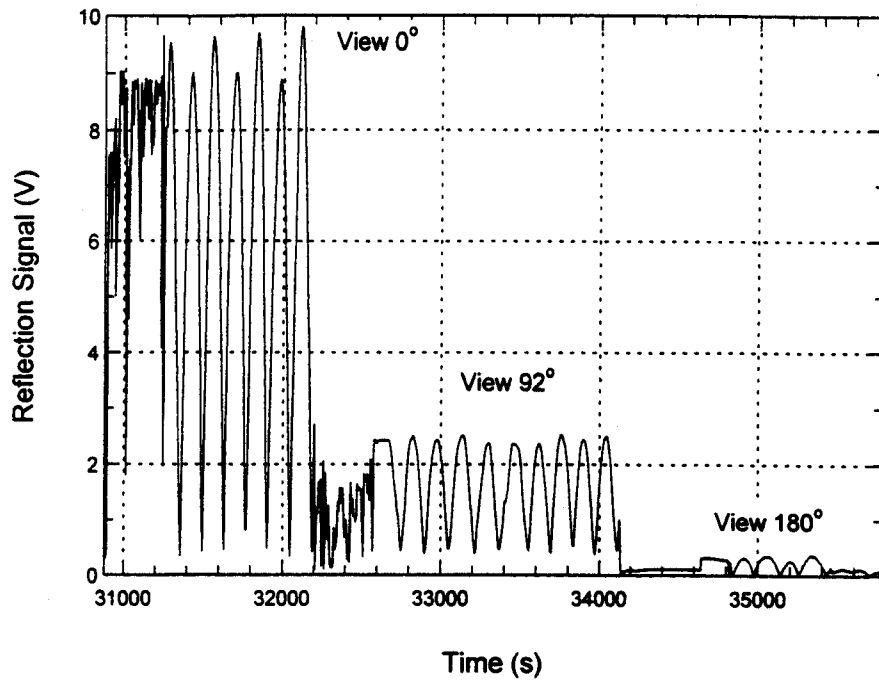


Figure 6. Typical reflection signals from inside Mark II with the pyrometer slowly translated along the signal path for three different views into Mark II.

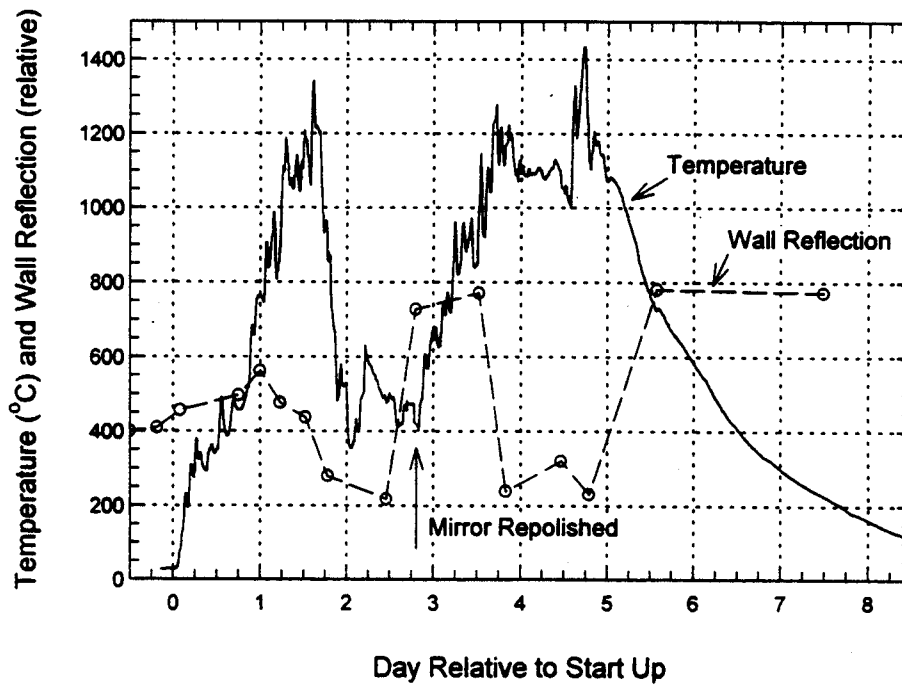


Figure 7. The complete temperature and wall reflection record for Mark II Run #3.

at about day 2.8, the graphite waveguide was pulled out of the furnace and the end mirror was found to have acquired a pitted powdery surface. It was repolished with fine emery cloth and reinstalled into the furnace. The return signal was significantly higher after the mirror was repolished and then decreased as the furnace warmed up again, but finally was found to have increased at the end of the run.

This was the only furnace run for which the wall reflectivity increased significantly between the start and end. It was also the first run after which the recessed flat reflecting surface in the wall was observed to have acquired a heavy coating of glass slag deposition. In addition, the waveguide mirror was observed to be corroded at the end of the run, similar to its appearance when it was pulled out at day 2.8. Post run calibration showed it to have degraded in reflectivity by about 20% relative to the start of the run. Adjusting the observed increase in the wall reflectivity for the measured mirror degradation implies that the surface reflectivity increased by a factor of 2.4 due to the surface deposition coating. This would correspond to a decrease in surface emissivity to 0.71 if we assume the starting emissivity was 0.88, the measured value for the high alumina content refractory surface when it was uncoated. However, closer examination of the reflection measurements indicates that there may be errors in this emissivity determination.

The observed increase in the reflection signal after the graphite mirror was repolished at day 2.8 is much higher than the measured 20% improvement in reflectivity accomplished by repolishing, even if we square it to account for the double pass of the probe beam off this mirror surface. There are many factors that can effect the reflection measurements besides degradation of the viewing mirror. Changes in relative alignment between the viewed surface and pyrometer is probably the most significant factor that could not be adequately adjusted for with only one axis of rotation for the waveguide/mirror system. Another factor is changes and drift in the local oscillator power used as the probe beam. Instrument refinements such as an independent measure of the transmission line losses, a monitor of the LO power, and additional adjustments for alignment and/or corner reflector refractory surfaces should make reflection measurements much more quantitative in the future.

VIII. Profile Measurements

The ability to make continuous surface profile temperature measurements inside a furnace with one small penetration is another important capability of the millimeter-wave pyrometer. Temperature gradients were found to exist inside the Mark II furnace throughout a run. Vertical cross section profiles recorded during Run #5 are shown in Figures 8 and 9 where the view direction axis corresponds to the directions shown in Figure 4. During warm up and at melt temperatures the ceiling is typically 200° to 400° C cooler than the hearth. Nonuniformities in the surface temperature across the fill inside the hearth also exist and are clearly resolved by the 5 cm spatial resolution of

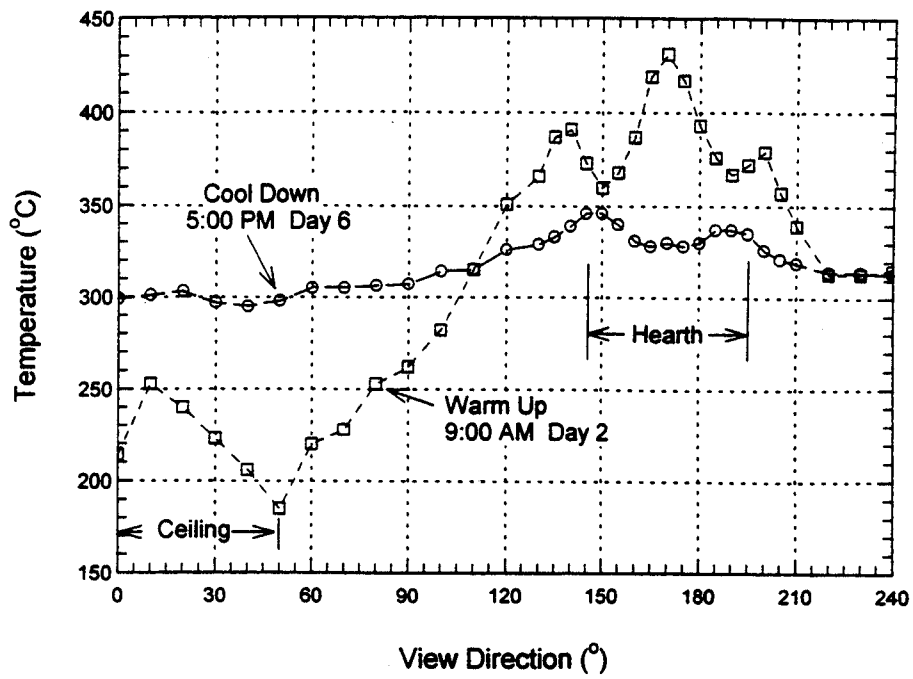


Figure 8. Temperature profiles inside Mark II during warm up and cool down for Run #5.

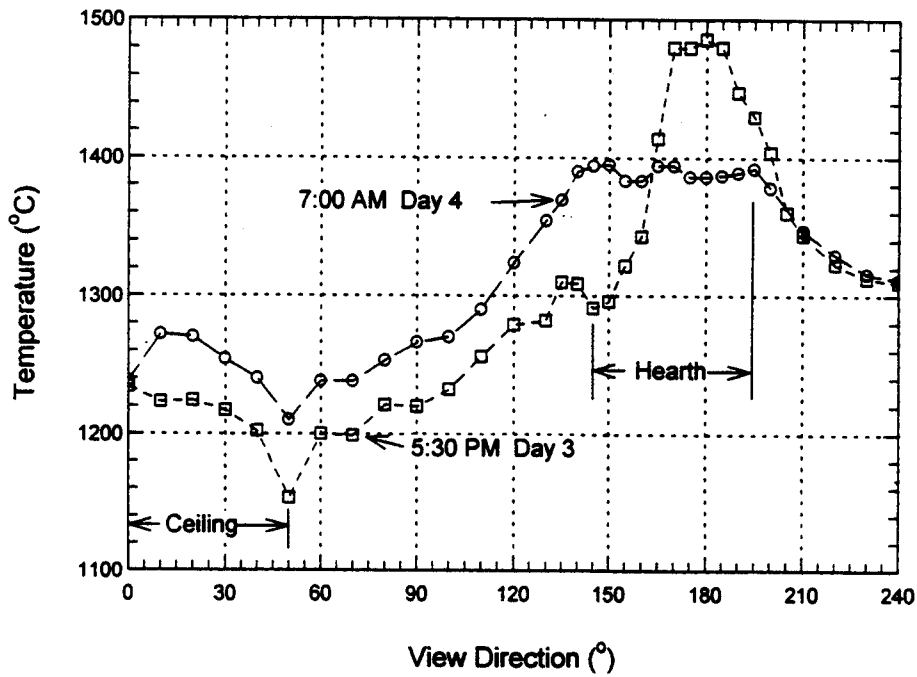


Figure 9. Temperature profiles inside Mark II at the highest temperature for Run #5.

the pyrometer. Temperature profile information such as this can be very useful for monitoring overall furnace performance and controlling the furnace process.

The spatial resolution of the pyrometer is demonstrated in profiles taken during warm up and cool down in Figure 8. Note the hot spot in the center of the hearth during warm up. The furnace was being joule heated through the center of the hearth and the pyrometer clearly resolved the higher temperatures there relative to the hearth edges. During cool down the temperature gradient inside Mark II is much smaller and a lower temperature is observed in the center of the hearth relative to the edges. This is reasonable since the thermal conductivity down through the graphite hearth would be faster during cool down than through the insulating refractory wall just above it.

Profiles taken during arcing and when the furnace was up at melt temperatures are shown in Figure 9. The trace for day 3 was made after the hearth was filled for the first time. A higher arc voltage made the hearth significantly hotter than the rest of the furnace. The off center appearance of the hot spot in the hearth is not necessarily real. It is most likely due to a slight upward drift in arc voltage during the scan across the hearth which took about 15 to 20 minutes to complete. Overnight the arc voltage was reduced and by next morning the profile scan shows a relatively uniform temperature across the entire melt surface. The furnace in general has also come up to a higher temperature. The capability of the pyrometer to determine the melt surface temperature uniformity was useful to confirm the readiness of the furnace for the second soil loading campaign.

The temperature profiles shown are not corrected for surface emissivity. Such a correction would increase the observed thermal gradients because the reflected component of the pyrometer field-of-view off the hottest surface would see a cooler surface and that off the coolest surfaces would see a hotter surface. A ray tracing analysis of where the reflected part of the pyrometer field-of-view is looking would need to be carried out to quantitatively account for surface emissivity.

That a surface emissivity of less than 1 is effecting the profile measurements is evident by a feature common to all the profiles. The coolest point is always at a viewing angle of 50° where the corner made by the ceiling and wall is viewed. This is probably caused by the millimeter-wave reflections being trapped in this corner so that the effective surface emissivity is always 1 in this view direction. When we look away from this corner up toward the ceiling part of the signal that gets to the pyrometer is by a reflection. The ceiling looks hotter because it sees the hearth by reflection.

The degree to how much hotter the ceiling looks relative to the corner has increased noticeably since the first run when the refractory surface was clean. This is illustrated in Figure 10 where a temperature profile taken during Run #1 is compared with one taken during Run #5 at roughly the same temperature during furnace warm up. Note the significantly higher ceiling temperature for approximately the same temperatures throughout the rest of the furnace. A calculation shows that the ceiling surface reflectivity would have to approximately double to account for the apparent increase in ceiling temperature relative to the corner. Correspondingly, the emissivity

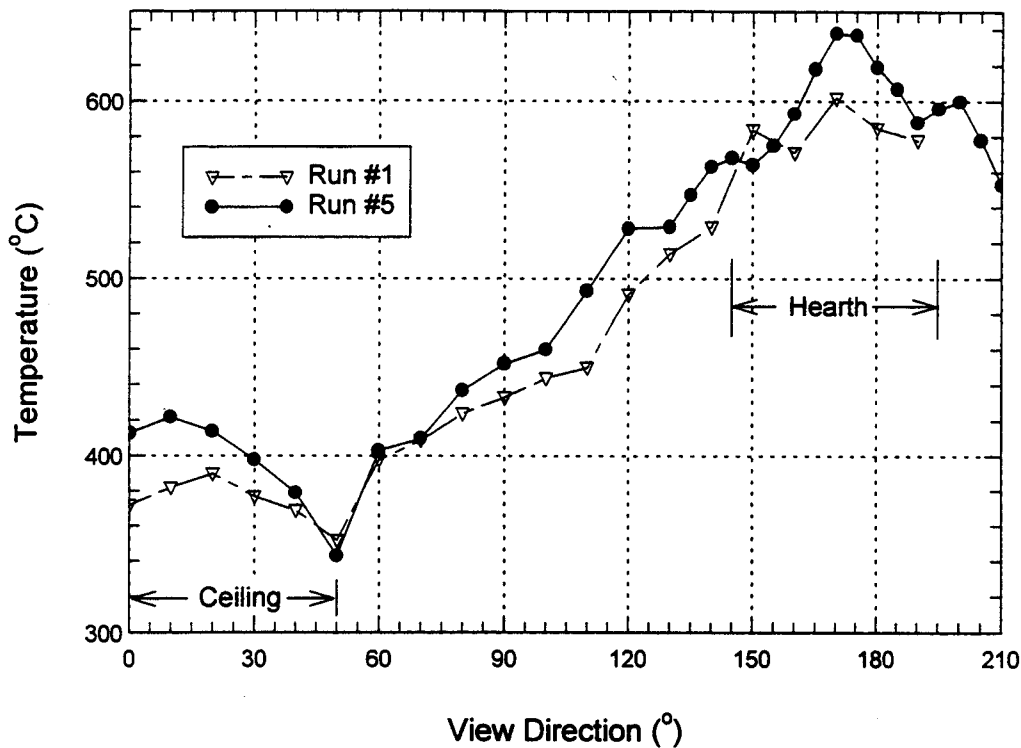


Figure 10. Comparison of temperature profiles inside Mark II during warm up for Run #1 and Run #5.

of the refractory surface would have had to change from 0.88 to about 0.76. This is in rough agreement with the decrease in surface emissivity observed with the reflection measurements above. It also demonstrates the usefulness of being able to take complete, continuous temperature profiles inside a furnace.

VIII. Conclusion

The active millimeter-wave pyrometer described here has proven to be a very capable and robust diagnostic instrument in a high temperature, dirty furnace environment. Real time, continuous temperature measurements were available from inside the Mark II DC graphite electrode arc furnace during five furnace runs with 24 hour pyrometer operation for more than a total of 30 days and reaching a maximum temperature of 2200° C. Smoke filled atmospheres inside the furnace were not observed to effect pyrometer performance. The active probing capability provided additional information on the condition of the internal furnace surfaces and on the losses in the pyrometer viewing optics. In particular, a potential capability to monitor changes in the surface emissivity was demonstrated for the first time, though future refinements in instrument implementation will be needed to improve accuracy.

The capability to fabricate efficient waveguides and mirrors from furnace refractory materials in the millimeter wavelength range has also been demonstrated. This allowed the implementation of a scanning mirror inside the furnace which made possible complete temperature profile measurements with only one small penetration into the furnace. Nonuniformities in the slag melt surface could be monitored and millimeter-wave light trapping corners could be observed as an independent check on reflection emissivity measurements. Pyrometer calibration remained robust even with corrosion of the internal graphite mirror because this corrosion occurs at high temperature and concurrent increased mirror emission largely compensates for the reduction in reflectivity. Corrosion of the graphite mirror could be eliminated in the future by the use of nonoxidizing coatings such as zirconium oxide or replacing this part of the waveguide with inconel.

The capabilities of an active millimeter-wave pyrometer for measurements inside a furnace are shown here to be significantly superior to currently available infrared pyrometers and thermocouples. This is accomplished with millimeter-wave electronics that do not need to be state-of-the-art. In fact noisier electronics are preferable for better temperature measurement linearity. The active probing capability is just a by product of the local oscillator leakage from a heterodyne receiver. With increasing availability of millimeter-wave components, active millimeter-wave pyrometry will undoubtedly become the technology of choice for measurements in many high temperature processes.

Acknowledgments

The support of this work by the Buried Waste Integrated Demonstration, Office of Technology Development, Environmental Demonstration and Waste Management, U. S. Department of Energy through Battelle - Pacific Northwest Laboratories under contract number 154462-A-L2 is gratefully acknowledged.

References

1. G. Taylor, P. C. Efthmion, M. McCarthy, E. Fredd, M. A. Goldman, and D. Kaufman, *Fast Scanning Heterodyne Receiver for the Measurement of the Time Evolution of the Electron Temperature Profile on the Tokamak Fusion Test Reactor*, Rev. Sci. Instrum., Vol. 56, pp. 928-930, 1985.
2. G. Smoot, C. Bennett, R. Weber, J. Maruschak, R. Ratliff, M. Janssen, J. Chitwood, L. Hilliard, M. Lecha, R. Mills, R. Patschke, C. Richards, C. Backus, J. Mather, M. Hauser, R. Weiss, D. Wilkinson, S. Gulkis, N. Boggess, E. Cheng, T. Kelsall, P. Lubin, S. Meyer, H. Moseley, T. Murdock, R. Shafer, R. Silverberg, and E. Wright, *COBE Differential Microwave Radiometers: Instrument Design and Implementation*, The Astrophysical Journal, Vol. 360, pp. 685-695, 1990.

3. J. E. Surma, D. R. Cohn, D. L. Smatlak, P. Thomas, P. P. Woskov, C. H. Titus, J. K. Wittle, and R. A. Hamilton, *Graphite Electrode DC Arc Technology Development for Treatment of Buried Wastes*, PNL-SA-21891, Pacific Northwest Laboratory, Richland, Washington, 1993.
4. J. H. Rainwater, *Radiometers: Electronic Eyes that see Noise*, *Microwaves*, pp. 58-62, September 1978.
5. R. Buschling, *Understanding and Applying IR Temperature Sensors*, *Sensors*, Vol. 11, pp. 32-37, 1994.
6. M. E. Tiuri, *Radio Telescope Receivers*, in Radio Astronomy, J. D. Krauss, McGraw Hill, New York, Chapter 7, 1970.
7. J. L. Doane, *Propagation and Mode Coupling in Corrugated and Smooth-Wall Circular Waveguides*, in Infrared and Millimeter Waves, Vol. 13, K. J. Button, Editor, Academic Press, Inc., New York, Chapter 5, 1985.
8. L. Rebuffi and J. P. Crenn, *Radiation Patterns of the HE₁₁ Mode and Gaussian Approximations*, *Intern. J. Infrared and Millimeter Waves*, vol. 10, pp. 291-311, 1989.
9. Manufactured by Emerson and Cuming.
10. J. Y. L. Ma and L. C. Robinson, *Night Moth Eye Window for the Millimetre and Sub-Millimetre Wave Region*, *Optica Acta*, 1983, vol. 30, p. 1685, 1983.
11. P. P. Woskov, D. R. Cohn, R. A. Hamilton, D. Y. Rhee, J. E. Surma, B. Sutharshan, P. Thomas, and C. H. Titus, *Initial Millimeter-Wave Radiometer Temperature Measurements Inside the Mark II Arc Furnace*, PFC/JA-94-1, Plasma Fusion Center, MIT, Cambridge, MA, 1994.